DOI: 10.61782/fa.2025.0790

FORUM ACUSTICUM
EURONOISE 2025

SOUND SOURCE IDENTIFICATION BASED ON BALANCE OF ACOUSTIC ENERGY

Johannes Kreuzinger[1*] **Florian Schwertfirm**[1]

[1] KM-Turbulenz GmbH, Rosenheimer Str. 67, 81667 Munich, Germnay

ABSTRACT

Using a hydrodynamic acoustic split approach to compute aeroacoustic sound provides acoustic quantities p^*, $\boldsymbol{u}^*$ in the complete domain, including the source region. Using these allows to compute the acoustic energy and it's balance terms. Production and dissipation of acoustic energy and acoustic intensity fluxes can be located and quantified.

The method used is the immersed boundary finite volume code MGLET, solving incompressible Navier-Stokes equations together with acoustic perturbation equations. In this CFD-CAA solver the terms are readily available and evaluated for an application case: a car HVAC outlet. The simulation of sound radiation is validated by comparison to measurements. For frequency bands at peaks in the sound spectra, the location and magnitude of production and dissipation of acoustic energy are analysed.

Keywords: *computational aeroacoustics, hydrodynamic/acoustic splitting, sound source identification, acoustic energy*

1. INTRODUCTION

To compute aeroacoustic noise, a widespread approach uses two sets of equations, one describing the flow and the other the acoustics, coupled by source terms, see [1] for an overview over different hybrid or split approaches and their application to car HVAC components. Main motivation is to facilitate the computation by using boundary conditions, grids or numerical approximations tailored for each equation set. In addition, the split of variables allows to analyse acoustic quantities in the source region delivering insight into the source mechanisms. In the present work the balance of acoustic energy is analyzed.

2. COMPUTATIONAL METHOD

The validated runtime coupled scale-resolving flow and acoustics solver MGLET [2] is used. This finite volume code is based on Cartesian hierarchical grids using a staggered variable arrangement with skew symmetric discretization of the convective term and a cut cell immersed boundary to represent arbitrary geometry. Implemented is a hydrodynamic/acoustic splitting approach [1] [3], where the incompressible Navier-Stokes equations describing the flow are coupled to acoustic perturbation equations by the source term $\frac{\nabla P'}{\rho_0}$. LES and wall models allow for the computation of turbulent flows at high Reynolds numbers.

3. APPLICATION CASE

The present case is a single car HVAC vent of a VW Passat, see Fig.1. An air flow of $0.0313\text{m}^3/\text{s}$ is supplied through a tube of 0.2m diameter, equipped with silencer and flow straightener. A converging section lined with sound absorbing foam connects the tube with the duct distributing the flow to right and left vent [2]. The right flow path is closed, only the left vent is present with a cross section around $100\text{mm} \times 40\text{mm}$ containing a throttle, 7 vertical and 3 horizontal fins. The duct and the vent are enclosed by a box (not shown), the opening is aligned with the vertical box wall. The radiated sound was measured at

*__Corresponding author__: j.kreuzinger@km-turbulenz.de.

[1] Notation used: Split of variable into sum of flow and acoustic variables: $a = A + a^*$; fluctuation around mean: a'.

[2] Left in the perspective of a car passenger (neg. y direction).

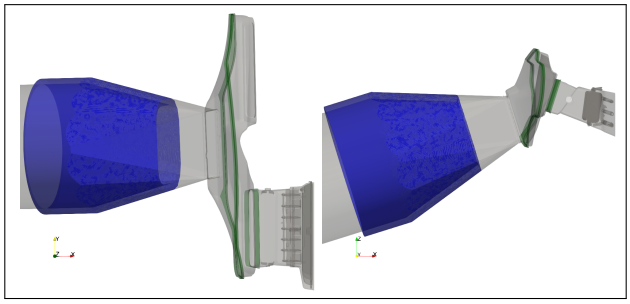

Figure 1. Geometry of the HVAC outlet.

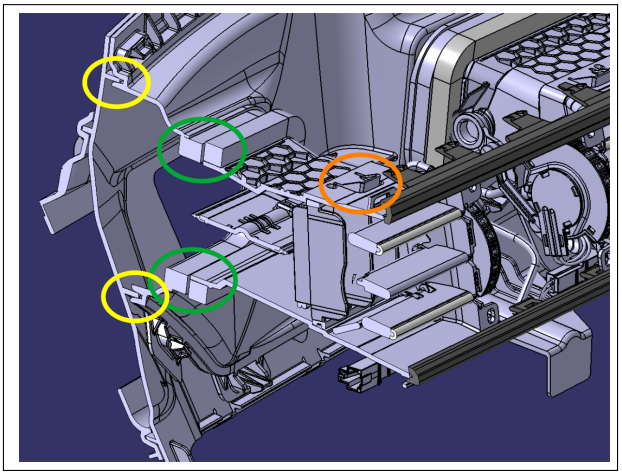

Figure 2. Details to be considered in the simulation.

4 microphones at 354mm distance from the center of the outlet in direction diagonal to the coordinate system. The spectra of these microphones are averaged.

The computational mesh has a grid spacing of 0.4mm in the outlet and 6.4mm between outlet and microphones, overall 44 million cells filling a domain of 8.5m^3. The Smagorinsky model is used for subgridscale stresses and the Werner-Wengle model for wall shear stress.

Special care has bee taken to correctly represent the acoustic boundary conditions. The foam in the converging section (blue in Fig.1.) is modeled as equivalent fluid with a Darcy coefficient according to measurements. At hard walls (grey in Fig.1.) thermal and viscous losses in the acoustic boundary layer are represented by a time domain version of the impedance given in [4]. Fig.2 shows positions, where the ducts are not perfectly tight and hard: 1st two parts sticked together (yellow), 2nd a closed cell foam sealing (green) and 3rd small holes (orange). The

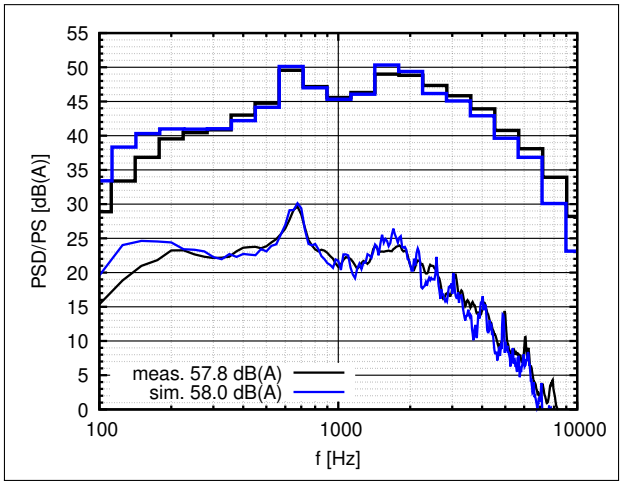

Figure 3. Sound spectra at microphones, measurement and simulation.

1st is modeled by a boundary condition representing the losses and transmission of a 0.1mm gap, the 2nd by a fixed absorption rate. This is visualized by the green boundary patches in Fig.1. The small holes (3rd) are resolved by the mesh.

The simulation predicts the radiated sound very well, see Fig.3. The narrow band PSD shows all peaks and the underlying noise level at correct amplitude and frequency compared to the measurement. For each 3rd octave between 200Hz and 6300Hz, measurement and simulation deviate less than 1.4dB. The summed up SPL matches by 0.2dB.

Accounting the losses at hard walls and the connections between the parts is essential to predict the radiated sound correctly. Neglecting them results in an increase of all resonance peaks up to 9dB and of the summed up SPL by 3dB, see Fig.4.

4. ACOUSTIC ENERGY BALANCE

The hydrodynamic/acoustic splitting approach provides separate fields describing the flow (P') and the acoustic quantities (p^*). Fig.5 shows these quantities projected on the surface of duct and nozzle. Although the amplitudes of the flow pressure surmount the acoustic pressure by more than one order of magnitude, the used splitting approach shows a clear separation of the flow pressure P' with small scale hydromechanic structures and the acoustic pressure p^* with its large scale acoustic waves. Using the acoustic

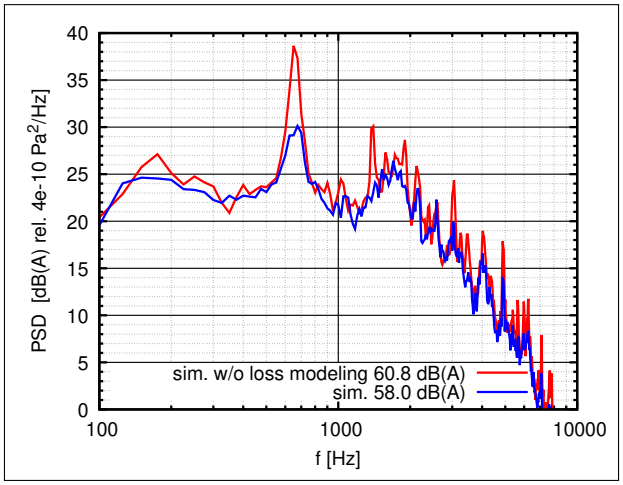

Figure 4. Sound spectra at microphones w/o and w/ losses of the duct.

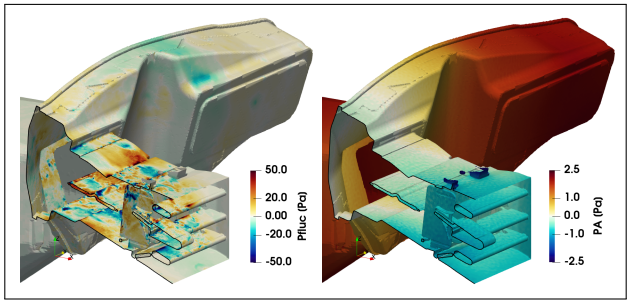

Figure 5. Left: Fluctuating incomp. pressure P'; Right: acoustic pressure p^*.

quantities it is possible to define an acoustic energy density [5]

$$e^* = \frac{1}{2}\frac{p^* p^*}{\rho_0 c_0^2} + \frac{1}{2}\rho_0 \boldsymbol{u}^* \cdot \boldsymbol{u}^* \tag{1}$$

and its balance equation. For the present application the balance of e^* neglecting convective terms and heat sources reads

$$\frac{\partial e^*}{\partial t} + \boldsymbol{\nabla} \cdot (p^* \boldsymbol{u}^*) = -\frac{p^*}{\rho_0 c_0^2}\frac{\partial P'}{\partial t} - D^* \tag{2}$$

The temporal change and the divergence of acoustic intensity constitute the LHS. The latter transports acoustic energy. The 1st term on the RHS is the production term describing energy transfer between flow and acoustics. It may be positive or negative, but mainly is positive. The

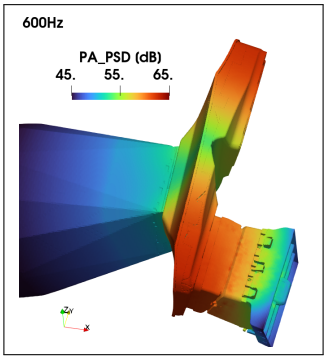

Figure 6. PSD of acoustic pressure p^*, frequency band 600Hz

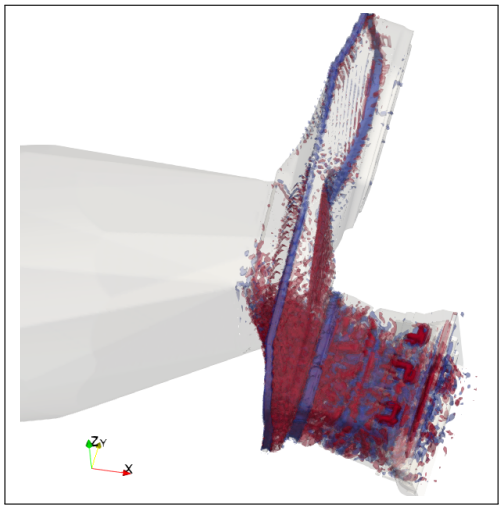

Figure 7. Isosurfaces of $\boldsymbol{\nabla} \cdot (p^* \boldsymbol{u}^*)$, frequency band 600Hz. Red/blue: pos./neg. values.

2nd term is the dissipation, which in the present case contains the losses in the absorbing foam. The divergence of the acoustic intensity can be regarded as net production with units $\mathrm{W/m^3}$. Its time average is equal to the averages of Production minus Dissipation.

In the following, the energy balance is used to analyse the sound at a 100Hz wide frequency band centered at 600Hz, corresponding to the dominant peak in the spectrum. Fig.6 shows the power spectral density of p^* at the surface for this band. An acoustic mode with two pressure bellies at the left an right end of the duct and a pressure node in the center is visible. $\lambda/2 = 28$cm fits roughly to the duct extension in y-direction of 38cm.

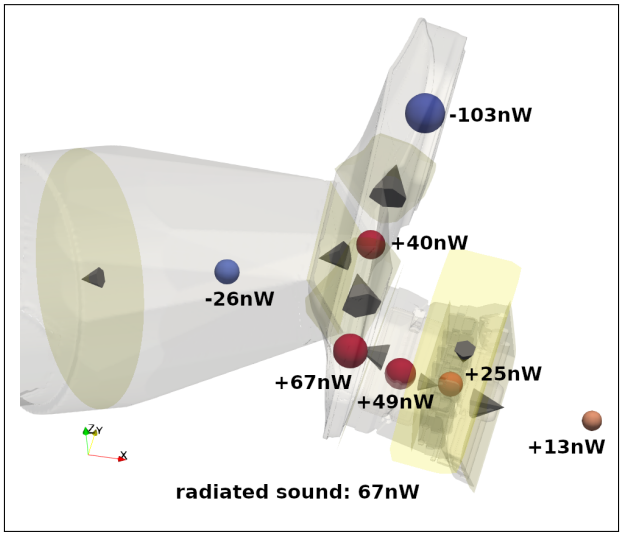

Figure 8. Integrated sound power production and sound power fluxes, frequency band 600Hz.

Strictly speaking $\mathrm{Re}\left(\widehat{p^*_{(k)}}\,\overline{\widehat{\boldsymbol{u}^*_{(k)}}}\right)$ at frequency band k is considered, but for the sake of simplicity, just $p^*\boldsymbol{u}^*$ is written. The field of $\boldsymbol{\nabla}\cdot(p^*\boldsymbol{u}^*)$ allows to locate sound sources. Fig.7 shows 20 isosurfaces of this quantity in the range $\pm 6\cdot 10^{-3}\mathrm{W/m^3}$. As the divergence in cells at the boundary is evaluated without the flux prescribed by the boundary condition, losses introduced by the BC show up as negative values of the divergence. The losses at the connections of the different duct parts appear as blue bands of negative values. In the left part of the duct and the vent high values are concentrated. Mostly it is positive production, partially also negative structures can be seen. The sign depends on the phase relation between p^* and P'.

Beyond this qualitative evaluation a quantitative analysis sheds additional light on the mechanisms involved in the sound production. The duct and nozzle are divided into sub-volumes, indicated by the transparent yellow planes in Fig.8. The integral net production $\int_V \boldsymbol{\nabla}\cdot(p^*\boldsymbol{u}^*)\,dV$ for each volume and the flux over the surfaces connecting the volumes $\int_S p^*\boldsymbol{u}^*\cdot d\boldsymbol{S}$ are computed for the frequency band, resulting in values of unit [W]. They are shown as spheres respectively cones, scaled with their magnitude. The highest values of net production appears at the 90 degree bend between duct and vent. Additional positive contributions are located in the center of the duct, in the vent and outside the vent, summing up to 194nW. This is mostly compensated by negative values in the dead end of the right side of the duct, due to viscous losses at the wall and in the gap at the connection between the two duct parts. This causes high values of sound power flux from the left to the right side of the duct. To a smaller extent there is also a power flux in upstream direction. Finally only 67nW, which is around 1/3 of sound power produced in the source regions, are radiated. This corresponds to a level of 48.3dB rel. 1pW. Considering radiation into a half space the sound pressure level at the microphone distance is 49.3dB rel.$(2{\cdot}10^{-5}\mathrm{Pa})^2$, fitting the 3rd octave value in the spectrum (Fig.3).

5. CONCLUSIONS

In case the boundary conditions are correctly modeled, a hydrodynamic/acoustic splitting approach solved by an energy conserving finite volume code can predict flow induced sound very accurate. Evaluation of the acoustic energy balance allows for quantitative analysis of both location and energy contribution of sound sources and sinks.

6. ACKNOWLEDGMENTS

We want to thank Simon Fischer from IAV in Chemnitz, Germany for sharing measurement results and geometry data with us.

7. REFERENCES

[1] M. Tautz, *Aeroacoustic Noise Prediction of Automotive HVAC Systems*. PhD thesis, Friedrich-Alexander-Universität Erlangen-Nürnberg, 2019.

[2] F. Schwertfirm, J. Kreuzinger, N. Peller, and M. Hartmann, "Validation of a hybrid simulation method for flow noise prediction," in *AIAA/CEAS Aeroacoustic Conference*, (Colorado Spring, USA), 2012.

[3] R. Ewert and J. Kreuzinger, "Hydrodynamic/acoustic splitting approach with flow-acoustic feedback for universal subsonic noise computation," *J. Comp. Physics*, vol. 444, no. 110548, 2021.

[4] M. Bruneau, P. Herzog, J. Kergomard, and J. D. Polack, "General formulation of the dispersion equation in bounded visco-thermal fluid, and application to some simple geometries," *Wave Motion*, vol. 11, pp. 441–451, 1989.

[5] S. Rienstra and A. Hirschberg, *An Introduction to Acoustics*. Eindhoven University of Technology, 2004.